

Accepted Manuscript

Corrosion and wear of PEO coated AZ91/SiC composites

B. Mingo, R. Arrabal, M. Mohedano, A. Pardo, E. Matykina

PII: S0257-8972(16)31037-4
DOI: doi:[10.1016/j.surfcoat.2016.10.041](https://doi.org/10.1016/j.surfcoat.2016.10.041)
Reference: SCT 21686

To appear in: *Surface & Coatings Technology*

Received date: 19 June 2016
Revised date: 21 September 2016
Accepted date: 14 October 2016



Please cite this article as: B. Mingo, R. Arrabal, M. Mohedano, A. Pardo, E. Matykina, Corrosion and wear of PEO coated AZ91/SiC composites, *Surface & Coatings Technology* (2016), doi:[10.1016/j.surfcoat.2016.10.041](https://doi.org/10.1016/j.surfcoat.2016.10.041)

This is a PDF file of an unedited manuscript that has been accepted for publication. As a service to our customers we are providing this early version of the manuscript. The manuscript will undergo copyediting, typesetting, and review of the resulting proof before it is published in its final form. Please note that during the production process errors may be discovered which could affect the content, and all legal disclaimers that apply to the journal pertain.

Corrosion and wear of PEO coated AZ91/SiC composites

B. Mingo^{a*}, R. Arrabal^a, M. Mohedano^a, A. Pardo^a, E. Matykina^a

^a*Departamento de Ciencia de Materiales, Facultad de Ciencias Químicas, Universidad Complutense, 28040 Madrid, Spain*

^{*}*Corresponding author. Tel: 34 91 3945227; Fax: 34 91 3944357*

E-mail: beatrizmingo@ucm.es

ABSTRACT

In this work, corrosion and wear resistance of uncoated and PEO coated AZ91/SiC/0-10p composites manufactured by semisolid processing is evaluated by corrosion tests in saline solution and *ball-on-disc* tests. AZ91/SiC composites show a globular microstructure with SiC clusters located at the interglobular regions. PEO coatings reveal a trilayered structure with thicker, less porous and softer regions at the locations of SiC clusters. Corrosion rate increases with increasing the volume fraction of reinforcement, which shows a cathodic activity and disrupts the continuity of the β -phase network. PEO improves the corrosion resistance, but it is also negatively influenced by the presence of the reinforcement. Tribological tests show a positive effect of the reinforcement on uncoated materials, whereas an opposite effect is found on PEO coated materials, probably due to the detachment of SiC particles from the coating.

KEYWORDS: Magnesium composite; Corrosion; Wear; SKPFM

1. INTRODUCTION

World production of magnesium has drastically increased during the last two decades, mainly due to its great potential in the transport industry, where weight reduction is a key factor in order to improve the economy of the vehicles. Magnesium has a low density (1.7 g cm^{-3}), high specific strength, good damping capacity, machinability and recyclability. However, it presents poor mechanical properties (strength and creep resistance) at high temperatures ($T > 120^\circ\text{C}$) and low corrosion resistance in aggressive environments, derived from its active nature and low tendency to form protective passive layers [1, 2]. These disadvantages limit the use of magnesium alloys to those parts of the vehicle which are not subjected to hostile environments (steering wheels, seat structures, dashboards...).

Alloy development is one of the most basic strategies to improve the performance of magnesium alloys. AJ62 (Mg-Al-Sr), MRI153M (Mg-Al-Ca), AE42 (Mg-Al-RE), ZE41 (Mg-Zn-RE) and ACM522 (Mg-Al-Ca-RE) are some examples of newly developed alloys which are used in power trains, gearbox housings or in valve covers, where good thermal stability and creep resistance are required [3-7]. However, alloy design cannot fulfill certain mechanical requirements demanded by the automotive industry which is one of the reasons of the increasing interest for magnesium based composites. SiC particles (SiC_p) are a common reinforcement phase in metal matrix composites since elastic modulus, yield strength, thermal stability, creep, wear and fatigue resistance can be significantly improved, although at the expense of a diminution of the corrosion performance [8-10]. The latter is often attributed to the formation of galvanic couples and/or to the heterogeneity of the matrix/ SiC_p interface [11].

Magnesium based composites reinforced with SiC_p are usually processed either in the liquid state or in the solid state. Although liquid state processes (i.e. stir casting, squeeze casting) are

relatively cheap and simple, they present a major limitation, which is the high reactivity between reinforcement and liquid matrix. This is especially important when Al is present in the alloy since Al carbide compounds (Al_4C_3) can be formed because of the high temperatures, which might affect negatively to the mechanical properties of the materials. Solid state processes, such as powder metallurgy, are preferred for manufacturing high volume fraction composites and stand out for their better performance in terms of interfacial reactions and reinforcement distribution, but they are normally time consuming [12]. During the last years, there has been a new trend to design alternative processing routes for metal matrix composites such as in-situ synthesis, friction stir processing and high-energy ball milling. Prominent among them is the semisolid-semisolid variation of compocasting, which differs from the more conventional semisolid-liquid variation on the state of the matrix (liquid or semisolid) during the casting stage. This processing route, in addition to lowering the operating temperatures (decreases interfacial reactions, extends die lifetime and enhances energy saving) allows laminar flow of the material (less shrinkage and porosity) [13, 14].

Despite these recent manufacturing developments, magnesium based composites usually require a surface treatment in order to minimize the negative effects of the reinforcement phase on corrosion resistance. Up to now, the most common surface treatments for improving the corrosion resistance of Mg based materials are chromate conversion coatings and anodizing due to their relative simplicity, high productivity and excellent results; however, the use of Cr^{6+} based compounds has been restricted by the European Chemical Agency due to their high environmental risk. Laser surface melting, electroplating and chromium free conversion coatings are capable of treating complex geometries with high control of the operation parameters, but result in coatings with relatively low thickness, which cannot provide enough corrosion and wear

protection in hostile environments. Thicker coatings with little environmental impact can be produced by gas-phase deposition processes (thermal spray coatings, PVD, CVD, etc.), however they are costly and require high deposition temperatures which might be detrimental for the substrate [15].

Plasma electrolytic oxidation (PEO) is an eco-friendly surface modification technique that derives from conventional anodizing, which is able to produce high performance and highly stable, thick ceramic coatings. PEO coatings are formed under DC or AC conditions, usually in alkaline electrolytes at high voltages leading to the formation of short-lived microdischarges [16]. The high current density at the location of the discharges results in an increased pressure (~ 100 MPa) and temperature ($\sim 2 \times 10^4$ K) which trigger chemical, electrochemical and plasma reactions and the subsequent formation of highly stable ceramic phases [17]. The resulting coatings have excellent hardness and adhesion which show better corrosion and tribological properties compared to films formed by conventional anodizing [18].

There is a relatively high number of studies concerned with PEO coatings on magnesium alloys [17, 18], but very few on magnesium matrix composites. In the latter materials, the morphology of the coating is affected by the presence of the reinforcing phase, usually SiC in the shape of particles, since its ceramic nature disrupts the continuity of the barrier layer, hinders the oxide growth and diminishes the efficiency of the process. How SiC particles behave during treatment depends on their specific dimensions and PEO electrical conditions as well as other parameters such as purity, amount and distribution [9, 11, 19, 20].

Even though PEO coatings have already demonstrated their potential to improve the surface properties of magnesium based composites [9, 11, 21, 22], to the best of the author's knowledge,

there are no published studies that evaluate the corrosion behaviour of untreated and PEO-treated Mg-based SiC_p composites manufactured by the semisolid-semisolid compocasting. The tribological response of these type of materials is also unknown, however, some studies related to the role of SiC particles incorporated into the PEO coating from the electrolyte, suggest a positive effect of the reinforcement phase [23]. In this work, PEO coatings on AZ91 alloy reinforced with 2, 5 and 10 % vol. SiC_p manufactured by semisolid-semisolid compocasting are studied from a corrosion and wear point of view by using electrochemical and hydrogen evolution measurements in naturally-aerated NaCl 3.5 wt.% aqueous solution and *ball-on-disc* tribological tests.

2. EXPERIMENTAL

2.1 Test materials

The materials studied in the present work were provided by Foundation CIDAUT (Spain). They were produced by using a commercial AZ91 alloy (wt.%: 9.15 Al, 0.007 Si, 0.002 Fe, 0.20 Mn, 0.003 Cu, 0.0005 Ti, 0.59 Zn, 0.001>Ni, Bal. Mg) electromagnetically stirred in the semisolid region at 625 °C and quenched in oil (semisolid-semisolid compocasting). Additions of 2, 5 and 10 vol. % of pretreated (8 h, 800 °C) SiC particles (15-25 µm) were made as required.

PEO coatings were obtained in a phosphate based electrolyte composed of 10 g/L, Na₃PO₄·12H₂O; 1 g/L KOH, 8g/L, NaF and 10 g/L CeO₂(0.56 µm particle size, 99.95% purity, Inframat Advanced Materials) under continuous agitation using a voltage-controlled EAC-S2000 power supply (ETsystems electronic) with a square electrical signal with a positive-to-negative pulse ratio of 390 V/−90 V at 500 Hz and a current density limit of 250 mA/cm² (rms). A KUSB-3116 Keithley data acquisition card (500 kS/s) was used to record voltage-time and

current-time dependencies. The PEO process lasted between 400 and 900 s, depending on the substrate, in order to achieve similar coating thicknesses for all the materials. Longer times were not used as they produced local burning during anodizing, particularly in high volume fraction composites. After the PEO treatment specimens were rinsed in purified water and dried in warm air.

2.2 Specimen preparation and characterization

The sample preparation for metallographic characterization was performed on longitudinal and cross section specimens. Samples were wet-ground through successive grades of silicon carbide abrasive paper and polished with diamond paste (0.1 μm finishing) using an ethanol based lubricant. In order to reveal the microstructure of the materials, specimens were etched with nital reagent (5 mL nitric acid + 95 mL ethanol) during 5 s, cleaned with isopropyl alcohol and dried in warm air.

Coated and un-coated specimens were examined by optical (Leica-Reichert MEF4M) and scanning electron microscopy (JEOL JSM-6400). The latter was equipped with an Oxford Link energy dispersive X-ray (EDS) microanalysis hardware. Microscopic characterization was carried out for all coated samples, but only cross-sections of AZ91 and AZ91/10SiC_p are presented here. Phase composition studies were performed by X-ray diffraction (XRD) using a Philips X'Pert diffractometer ($\text{CuK}\alpha = 1.54056 \text{ \AA}$). The XRD patterns were registered for 2θ values between 10° and 90° (step size 0.04 and time per step 5 s) at a glancing angle of 0.5° .

A Fischer ISOSCOPE FMP10 portable instrument was used to measure the coating thicknesses by the eddy-current method, taking the average of ten measurements with a standard deviation of $<0.5 \text{ mm}$ and later confirmed with cross-sectional scanning electron microscopy (SEM). Surface

roughness was measured in five different locations with a Surtronic25 tester (Taylor Hobson Precision).

Hardness of uncoated materials was evaluated using a Vickers AKASHI AVK–AII and KASHIMVK-E3 instruments respectively. For the untreated materials, a 5 kg load was used during 20 s. This was done in order to produce a relatively large indentation area with contribution of all constituents present in the composite materials. For the coatings, a 25 g load was used during 20 s in cross-section specimens so as to determine the hardness of the coating without influence of the substrate.

Surface potential measurements were carried out in a Nanoscope IIIa MultiMode scanning Kelvin probe force microscope (SKPFM) in tapping mode on polished specimens. Topographic and surface potential images were acquired simultaneously using a Pt coated Si tip (OSCM-Pt) using the two-pass technique keeping the tip-sample distance constant at 100 nm. All measurements were performed at room temperature with a relative humidity of 30-40 %.

2.3 Corrosion tests

Hydrogen evolution tests were carried out by triplicate during 8 days of immersion in aqueous 3.5 wt.% NaCl solution at $(22 \pm 1)^\circ\text{C}$ with a working area limited to $\sim 1.5\text{ cm}^2$. Figure 1 shows the experimental set-up used for collecting the H_2 gas generated during the corrosion process.

Corrosion rate, P ($\text{mg cm}^{-2} \text{ d}^{-1}$), was calculated using expression (1) which links the H_2 volume evolved in the cathodic reaction, V_{H_2} (mL), with the magnesium mass dissolved in the anodic reaction for an exposed area A (cm^2) and time t (days) [24, 25].

$$P = \frac{1.085V_{\text{H}_2}}{A t} (1)$$

The electrochemical measurements were performed using an AUTOLAB computer-controlled potentiostat (PGSTAT 30) in naturally aerated 3.5 wt. % NaCl (pH 6.5) solution at $\sim 23^{\circ}\text{C}$, using a three-electrode cell. The test material served as working electrode (immersed area 1 cm^2) and a graphite and silver/silver chloride (Ag/AgCl 3M) as the counter and reference electrodes, respectively. The cathodic and anodic branch of the polarization curves of AZ91/SiC/0-10p were obtained in two separate experiments [26] after 1 h of immersion, at a scanning rate of 0.3 mV/s , starting from -150 mV vs. the open circuit potential (OCP) to the OCP (cathodic curve) and from the OCP until a maximum current of 5 mA/cm^2 (anodic curve). PEO coated potentiodynamic curves were obtained in one experiment, using the similar scan rate, starting from -150 mV vs. the OCP until a maximum current of 5 mA/cm^2 . Electrochemical tests were performed at least twice in order to ensure reproducibility.

Characterization of the corrosion products was carried out after the hydrogen evolution tests by SEM, optical microscopy and low-angle X-ray diffraction by using the same operating conditions described in Section 2.2.

2.4 Wear tests

Wear tests were performed in a MT/60/Ni ball-on-disc tester (MicroTest), using an AISI 52100 ball of 6 mm in diameter as counterpart. Tests were carried out at different sliding distances (100, 250, 500, 1000 and 1500 m) at 5 N and 200 rpm. The radius of the track was 3 mm. Plan view and cross section of the tested specimens were characterized by SEM with the aim of identifying the dominant wear mechanism. Experiments were carried out by triplicate.

3. Results and discussion

3.1 Characterization

3.1.1 Characterization of un-coated materials

Figure 2a shows the SEM micrograph of AZ91 magnesium alloy where a globular microstructure of the α -Mg phase and a partially divorced eutectic α -Mg_{eut}/ β -Mg₁₇Al₁₂ located in the interglobular region, creating an interconnected continuous network, can be observed. Al-Mn (Al₈Mn₅) inclusions of ~14 μ m average diameter are identified within the matrix and at the eutectic regions. A similar microstructure is found in composite materials AZ91/SiC_p, but with the incorporation of SiC_p clusters located in the interglobular regions (Figure 2b-f). This resulted in increased hardness values for the composite materials (Table 1). Al₈Mn₅ inclusions are also identified, but in this case, unlike in AZ91 alloy, they are slightly agglomerated (Figure 2f).

It is worth mentioning that no chemical reaction between the reinforcement phase and the matrix is identified as deduced from the absence of metal carbides. Mg carbides are not commonly formed since they tend to decompose at low temperatures (MgC₂, 500°C and Mg₃C, 650°C). However the formation of Al based carbides (Al₄C₃ and Al₂MgC₂) is quite common during the manufacturing of metal matrix composites due to the high reactivity of Al with C, and this is detrimental for the material performance, since these types of compounds are unstable in humid environments and could result in the formation of crevices around the reinforcing phase [27].

The lack of Al carbides in the studied materials can be related to the lower temperatures used during the manufacturing (semisolid-semisolid compocasting) compared to the ones reached in liquid state processing methods.

Surface potential maps of the different phases present in the studied materials were obtained by scanning Kelvin probe force microscopy. AZ91 and AZ91/SiC/5p surface potential maps and their profiles are collected in Figure 3. All phases showed a cathodic behaviour with respect to

the α -Mg matrix, being in the range of 130-240, 160-300 [28] and 400-500 mV for β -Mg₁₇Al₁₂, Al-Mn and SiC_p respectively. Surface potential measurements on AZ91 magnesium alloys have been performed by several authors and differing values have been reported. For instance, β -phase and Al-Mn potentials compared to the α -Mg matrix vary from ~30 mV and ~220 mV in an extruded AZ91 [1] to ~250 mV and ~380 mV in a die cast AZ91 alloy [29], respectively. This is attributable to compositional differences resulting from the processing route or the thermal history of the alloy. For instance, higher cooling rates lead to a greater Al segregation within the α -Mg matrix, which results in the formation of more intense galvanic couples. In case of SiC particles SKPFM measurements are scarce. For instance Pardo, in a A360/SiC_p obtained a potential difference of ~ 1000 mV with respect to the aluminium matrix [30].

3.1.2 Voltage/Current signals during PEO

Voltage and current-time dependencies of AZ91/0-10p-PEO are shown in Figure 4 where two different tendencies can be observed. The difference between unreinforced and reinforced materials is observed as early as 50 s, the voltage being slightly lower for reinforced materials. AZ91/0-2p-PEO show a current drop after 200 and 240 s respectively, indicating the formation of coatings with relatively high impedance. On the contrary, no current drop is observed for AZ91/5-10p-PEO during the applied treatment time. This behaviour and the lower voltage slope for the composite materials suggest that SiC particles in the substrate break the continuity of the barrier layer that forms on PEO coatings, delaying the passivation of the metal surface. Similar features were observed by Wang [19].

3.1.3 Characterization of PEO coated materials

The cross section of the PEO coated AZ91 alloy is shown in Figure 5a. It presents a cratered morphology, roughness of R_a (2.1 ± 1.8) μm and R_z (18.3 ± 0.8) μm , thickness of ~55 μm and

hardness of $\sim 300 \text{ HV}_{0.025}$. It presents a trilayered structure formed by a nanometric barrier layer and intermediate and external layers with pores of variable size. The incorporated CeO_2 particles, added to the electrolyte in order to improve the corrosion resistance [31], are easily identified in the outer region of the coating by their higher contrast in the BSE micrographs (Figure 5a). The specific mechanism of particle incorporation from the electrolyte is not completely understood and there are several approaches that try to explain it. It may occur through a simple physical deposition over the coating, by field assisted electrophoresis or by a mechanical entrapment by the molten metal [32, 33], although, it probably occurs by a combination of the three. The main constituents of the coatings, obtained by XRD analysis, are MgO , Al_2O_3 , MgF_2 and CeO_2 (Figure 6). The presence of the latter indicates inert incorporation of CeO_2 particles into the coating possibly due to their high melting point (2400°C). According to EDX analysis there is also P in the coating (below 10 at.%) possibly in the form of amorphous constituents.

PEO coatings on AZ91/ SiC_p composites are more heterogeneous and show a wider range of thicknesses ($55\text{--}80 \mu\text{m}$). The heterogeneities are mainly associated with the presence of SiC_p clusters which increase considerably the surface roughness (Table 2). At the locations of these clusters the coating has a completely different nature; it is denser, thicker ($\sim 80 \mu\text{m}$), but also softer ($\sim 80 \text{ HV}_{0.025}$), probably due to the presence of a high number of microcracks (Figure 5b) formed as a consequence of thermal stresses [34]. Additionally, there is a higher amount of F (Location 1, at. %: 53.0 –F, 23.0–Mg, 1.5–P; Location 2, at. %: 27.2–F, 33.9–Mg, 29.1–O, 5.2–P, Figure 5c), most likely in the form of MgF_2 as shown in XRD results, and a limited incorporation of CeO_2 particles in these areas (Figure 5c and 5d). All of these features, in particular the greater thickness, are believed to be associated with the presence of SiC breaking up the continuity of the barrier layer and, therefore, facilitating a higher number of discharges in

these regions. Once SiC particles are completely incorporated into the coating, the barrier layer recovers its homogeneity and discharges occur somewhere else on the surface. The high temperature and pressure generated at the location of the discharges often result in oxidation of SiC particles (as shown in Figure 7), which has been previously observed in similar materials [21, 35]. The reason for the limited inward mass transfer of CeO_2 particles is not clear; it is possible that a different type of discharges is responsible for this. For instance, a transition to the “soft sparking” regime could explain the limited incorporation of suspended particles from the electrolyte due to the formation of narrower discharge channels [32].

3.2 Corrosion tests

3.2.1 Hydrogen evolution tests

Corrosion rates of AZ91/SiC_p and AZ91/SiC_p-PEO calculated from H₂ evolution tests are represented in Figure 8. Non-reinforced AZ91 alloy presents an extraordinary corrosion resistance with values much lower than those of as cast or die cast AZ91 magnesium alloys [36]. This behaviour was recently explained by the authors in [28] and was attributed to the continuity of the $\beta\text{-Mg}_{17}\text{Al}_{12}$ (β -phase) boosting its barrier effect against corrosion, despite its cathodic behaviour (Figure 3a).

As shown in Figure 8, there is a clear negative influence of SiC_p incorporation on the corrosion behaviour of AZ91 alloy. This is usually associated with the heterogeneity at the matrix/reinforcement interface [9, 11, 37] and less frequently with galvanic corrosion phenomena [30]. PEO coated materials usually show better corrosion resistance compared to the uncoated materials; this is attributable to the formation of a thin and highly protective barrier layer at the substrate/coating interface [11, 38, 39]. This is the case for the unreinforced AZ91

and AZ91/SiC/2-5p PEO coated composites, which show corrosion rates 2-7 times lower compared to uncoated materials. However, increasing values of corrosion rate are observed as the SiC_p content increases, evidencing the detrimental effect of reinforcement incorporation on the corrosion resistance of coated materials. This negative response is possibly associated with the breakdown of the inner barrier layer caused by the presence of SiC_p, which impedes the homogeneous growth of the latter.

3.2.2 Electrochemical tests: Potentiodynamic curves

Figure 9a shows the polarization curves of uncoated AZ91/SiC_p after 1 h of immersion, where it can be observed a negligible influence of the reinforcement in the corrosion potential ($E_{\text{corr}} \sim -1.55 \text{ V}_{\text{Ag/AgCl}}$) and in the kinetics of the anodic reaction. The rapid increase in current density in the anodic range and the proximity, in all cases, between E_{corr} and E_{bd} (breakdown potential) suggests that the materials are locally corroded at the corrosion potential, although the slightly steeper slope of unreinforced material evidences a lower tendency for localized corrosion. On the contrary, the kinetics of the cathodic reaction is indeed influenced by the reinforcement proportion. According to the cathodic branches of the polarization curves, higher cathodic currents are found when increasing the SiC_p volume fraction; this evidences that galvanic corrosion at the SiC/ α -Mg interface is likely to occur in the studied composites. This effect combined with the disrupted continuity of the β -phase at the location of SiC particles explains the poor corrosion resistance of these materials.

Figure 9b gathers the potentiodynamic response of PEO coated composites. AZ91-PEO shows a $E_{\text{corr}} = -1.58 \text{ V}$ and a passive region of $\sim 70 \text{ mV}$; the incorporation of increasing amounts of SiC_p slightly shifts the E_{corr} towards more noble potentials and shifts the current density up to two

orders of magnitude higher. Additionally, the passive region disappears, probably due to the damage of the barrier layer caused by the presence of disrupting SiC particles at the interface between barrier layer and substrate. Figure 9c, compares the current density values of uncoated and PEO coated materials vs SiC_p vol. %, where it can be observed that for AZ91/0-5p, PEO coated specimens present higher corrosion resistance. However, in case of AZ91/10p an opposite behaviour is found, which can be associated with a more aggressive localized corrosion phenomenon that might occur derived from the local breakdown of the coating.

3.2.3 Surface appearance and characterization of corrosion

The cross section of the uncoated materials after 8 days of immersion in naturally-aerated NaCl 3.5 wt. % solution is shown in Figure 10. It can be observed for all the materials that the corrosion progresses through the α -Mg matrix, remaining the β -phase unattacked. However, it is evident in Figure 10b and 10c that SiC particles interrupt the continuity of the β -phase, hindering therefore, its barrier effect against corrosion. This explains in part the lower corrosion resistance of composites compared to the unreinforced alloy. XRD analysis of the corroded surfaces (not shown here) indicate that the main corrosion products are brucite and hydrotalcite [28].

In case of PEO coated composites, the cross-sections reveal corrosion damage at the coating/substrate interface (Figure 11) [27], and it is localized at the SiC_p rich regions, as deduced from the partial substrate dissolution and accumulation of small amounts of corrosion products. Therefore, corrosion initiation is probably related to the SiC particles disturbing the barrier layer. Consequently, higher volumetric percentage of reinforcement phase results in a greater damage of the barrier layer, leading to lower corrosion resistance of the coatings.

3.3 Wear test

The uncoated materials demonstrated a direct relationship between the surface hardness and the friction coefficient which were increasing with the particle content from HV₅ 82 to HV₅ 133 and from 0.34 to 0.54, respectively. Wear mass losses as a function of the sliding distance of AZ91/SiC_p composites follow a linear behaviour with smaller slopes for increasing amounts of SiC_p (Figure 12a). The wear resistance of magnesium based composites mainly depends on two factors, size and volume fraction of the reinforcing phase [12, 40]. The high stress concentration at the tips of the SiC particles contributes to the emergence of dislocations around the reinforcement decreasing the ductility [41] and increasing the hardness and strength, therefore resulting in a greater resistance against plastic deformation of the matrix [42]. Obviously, this behavior becomes more evident for higher reinforcement concentrations, which results in lower wear kinetics.

The wear resistance of the AZ91/SiC/0-10p composites is significantly improved with PEO coatings as deduced from the significantly lower mass loss values (Figure 12b). However, contrary to non-coated materials, increasing the SiC_p fraction in PEO coated composites results in a greater wear mass loss. This negative effect is clearly observed in AZ91/SiC/5-10p composites which fail at sliding distances below 100 m, with the complete removal of PEO coating from the surface and consequent establishment of metal-to-metal contact [43]. This can be explained by the additional abrasive effect caused by detached particles from the coating [44]. In a similar study by Yan [45], it was found that the incorporation of SiC nanoparticles to the coating from the electrolyte improved the wear resistance. This suggests that the size of the reinforcement is a key factor in the wear response of PEO coated composites; relatively big particles, as the ones used in this work (15-25 μm), are detached easily compared to nanoparticles which are intimately integrated within the coating. The removed particles act as a

third body influencing negatively the overall wear response of the material, due to their further abrasive effect.

Wear tracks were examined by SEM on longitudinal and cross-section specimens. For non-coated materials, there is a clear reduction in track depth with increasing amounts of SiC_p (Figure 13a). However, the track width remains almost constant (Figure 13b), which is indicative of significant wear of the steel counterpart. The wear track of the unreinforced alloy reveals parallel grooves or ploughing lines which are the main feature of an abrasive wear mechanism between the hard steel counterpart and the softer magnesium matrix. Additional wear mechanisms include adhesion and oxidation, marked by arrows in Figure 14a and 14b. Reinforced materials showed similar wear mechanisms (Figure 14c and 14d), but with greater adhesion features coming from the steel counterpart, as revealed by EDS analysis performed in the area marked with a cross in Figure 14c (52.1O-39.3Mg-3.5Al, 2.0Si-0.1Cr-3.1Fe). Figure 15 shows the longitudinal and cross section views of the wear track of PEO coated AZ91/SiC/2p. Owing to the high hardness of the PEO coating the steel ball wears down forming a Fe-rich transfer layer on the surface, which shows microcracks and signs of delamination (Figure 15b). It is believed here that poor cohesion of the coatings facilitates its delamination and therefore, their failure. These features are similar for the other studied materials.

4. Conclusions

- AZ91/SiC_p composites show a globular microstructure with an interconnected β -phase network, Al-Mn inclusions and SiC particles in the form of clusters that are located at the interglobular regions. PEO coatings show a trilayered structure with thicker, less porous and softer regions at the locations of SiC clusters.

- Corrosion rate of uncoated AZ91/SiC_p composites increases with increasing volume fraction of reinforcement. This has been attributed to the heterogeneous α -Mg/SiC interfaces, the cathodic behaviour of SiC particles and their detrimental effect on the continuity of the β -phase. The corrosion resistance of AZ91/SiC_p composites is improved with PEO coatings, but there is a clear negative influence of the reinforcement.
- Wear resistance of AZ91/SiC_p increases with the reinforcement volume fraction. PEO coatings improve further the tribological properties of the studied composite materials, however in this case the reinforcement phase influences negatively the wear resistance of PEO coated materials, possibly, due to abrasive effect of detached SiC particles.

Acknowledgements. The authors are grateful to MINECO/FEDER (Spain, Project MAT2015-66334-C3-3-R) for financial support and to the Community de Madrid (Spain, MULTIMATS2013/MIT-2862). E. Matykina is grateful to the MICINN (Spain) for financial support via the Ramon y Cajal Programme (RYC-2010-06749).

5. References

- [1] R. Arrabal, E. Matykina, A. Pardo, M.C. Merino, K. Paucar, M. Mohedano, P. Casajús, Corrosion behaviour of AZ91D and AM50 magnesium alloys with Nd and Gd additions in humid environments, *Corros. Sci.*, 55 (2012) 351-362.
- [2] R. Arrabal, A. Pardo, M. Merino, M. Mohedano, P. Casajús, K. Paucar, G. Garcés, Effect of Nd on the corrosion behaviour of AM50 and AZ91D magnesium alloys in 3.5 wt.% NaCl solution, *Corros. Sci.*, 55 (2012) 301-312.
- [3] G. L'Espérance, P. Plamondon, M. Kunst, A. Fischersworring-Bunk, Characterization of intermetallics in Mg-Al-Sr AJ62 alloys, *Intermetallics*, 18 (2010) 1-7.
- [4] G. Gertsberg, N. Nagar, M.B.B. Lautzhe, N. Moscovitch, S. Schumann, Effect of HPDC parameters on the performance of creep resistant alloys MRI153M and MRI230D, *SAE Tech. Publ.*, SAE, (2005).
- [5] T. Rzychoń, A. Kielbus, Effect of rare earth elements on the microstructure of Mg-Al alloys, *JAMME*, 17 (2006) 149-152.

- [6] Z. Yang, J. Li, J. Zhang, G. Lorimer, J. Robson, Review on research and development of magnesium alloys, *Acta Metall. Sin.*, 21 (2008) 313-328.
- [7] O. Gaon, B. Kazanski, A. Lugovskoy, Corrosion Behavior of MRI153M Magnesium Alloy in 3% NaCl Solution, *Solid State Phenomena*, Trans Tech Publ, 2015, pp. 83-86.
- [8] M.J. Shen, M.F. Zhang, W.F. Ying, Processing, microstructure and mechanical properties of bimodal size SiCp reinforced AZ31B magnesium matrix composites, *Journal of Magnesium and Alloys*, 3 (2015) 162-167.
- [9] W. Xue, Q. Jin, Q. Zhu, M. Hua, Y. Ma, Anti-corrosion microarc oxidation coatings on SiCP/AZ31 magnesium matrix composite, *J. Alloys Compd.*, 482 (2009) 208-212.
- [10] M. Fine, J. Weertman, Tailored interfaces for metal-matrix composites-fundamental considerations. Final technical report, 1 October 1988-30 November 1992, Northwestern Univ., Evanston, IL (United States). Dept. of Materials Science and Engineering, 1993.
- [11] R. Arrabal, A. Pardo, M. Merino, M. Mohedano, P. Casajús, E. Matykina, P. Skeldon, G. Thompson, Corrosion behaviour of a magnesium matrix composite with a silicate plasma electrolytic oxidation coating, *Corros. Sci.*, 52 (2010) 3738-3749.
- [12] N. Chawla, K.K. Chawla, *Metal Matrix Composites*, Springer Science & Business Media 2013.
- [13] F. Akhlaghi, A. Lajevardi, H.M. Maghanaki, Effects of casting temperature on the microstructure and wear resistance of compocast A356/SiCp composites: a comparison between SS and SL routes, *J. Mater. Process. Technol.*, 155-156 (2004) 1874-1880.
- [14] H. Khosravi, F. Akhlaghi, Comparison of microstructure and wear resistance of A356-SiCp composites processed via compocasting and vibrating cooling slope, *T Nonferr. Metal. Soc.*, 25 (2015) 2490-2498.
- [15] J. Creighton, P. Ho, Introduction to chemical vapor deposition (CVD), *Chem. Vap. Deposition*, 2 (2001) 1-22.
- [16] E. Matykina, R. Arrabal, A. Mohamed, P. Skeldon, G.E. Thompson, Plasma electrolytic oxidation of pre-anodized aluminium, *Corros. Sci.*, 51 (2009) 2897-2905.
- [17] T.S. Narayanan, I.S. Park, M.H. Lee, Strategies to improve the corrosion resistance of microarc oxidation (MAO) coated magnesium alloys for degradable implants: Prospects and challenges, *Prog. Mater. Sci.*, 60 (2014) 1-71.
- [18] F. Walsh, C. Low, R. Wood, K. Stevens, J. Archer, A. Poeton, A. Ryder, Plasma electrolytic oxidation (PEO) for production of anodised coatings on lightweight metal (Al, Mg, Ti) alloys, *Transactions of the IMF*, 87 (2009) 122-135.
- [19] Y.Q. Wang, X.J. Wang, W.X. Gong, K. Wu, F.H. Wang, Effect of SiC particles on microarc oxidation process of magnesium matrix composites, *Appl. Surf. Sci.*, 283 (2013) 906-913.
- [20] S.-y. Wang, N.-c. Si, Y.-p. Xia, L. Liu, Influence of nano-SiC on microstructure and property of MAO coating formed on AZ91D magnesium alloy, *T Nonferr. Metal. Soc.*, 25 (2015) 1926-1934.
- [21] R. Arrabal, E. Matykina, P. Skeldon, G.E. Thompson, Coating formation by plasma electrolytic oxidation on ZC71/SiC/12p-T6 magnesium metal matrix composite, *Appl. Surf. Sci.*, 255 (2009) 5071-5078.
- [22] Y.Q. Wang, M.Y. Zheng, K. Wu, Microarc oxidation coating formed on SiCw/AZ91 magnesium matrix composite and its corrosion resistance, *Mater. Lett.*, 59 (2005) 1727-1731.
- [23] L. Yu, J. Cao, Y. Cheng, An improvement of the wear and corrosion resistances of AZ31 magnesium alloy by plasma electrolytic oxidation in a silicate-hexametaphosphate electrolyte with the suspension of SiC nanoparticles, *Surf. Coat. Technol.*, 276 (2015) 266-278.
- [24] G. Song, A. Atrens, Understanding magnesium corrosion—a framework for improved alloy performance, *Adv. Eng. Mater.*, 5 (2003) 837-858.
- [25] G. Song, A. Atrens, D. StJohn, An Hydrogen Evolution Method for the Estimation of the Corrosion Rate of Magnesium Alloys, *Magnesium Technology 2001*, 254-262.
- [26] M. Curioni, The behaviour of magnesium during free corrosion and potentiodynamic polarization investigated by real-time hydrogen measurement and optical imaging, *Electrochim. Acta*, 120 (2014) 284-292.

- [27] C. Liu, J. Liang, J. Zhou, Q. Li, Z. Peng, L. Wang, Characterization and corrosion behavior of plasma electrolytic oxidation coated AZ91-T6 magnesium alloy, *Surf. Coat. Technol.*, 304 (2016) 179-187.
- [28] B. Mingo, R. Arrabal, M. Mohedano, A. Pardo, E. Matykina, A. Rivas, Enhanced Corrosion Resistance of AZ91 Alloy Produced by Semisolid Metal Processing, *J. Electrochem. Soc.*, 162 (2015) C180-C188.
- [29] M. Jönsson, D. Thierry, N. LeBozec, The influence of microstructure on the corrosion behaviour of AZ91D studied by scanning Kelvin probe force microscopy and scanning Kelvin probe, *Corros. Sci.*, 48 (2006) 1193-1208.
- [30] A. Pardo, M. Merino, M. Lopez, F. Viejo, M. Carboneras, S. Merino, Influence of reinforcement grade and matrix composition on corrosion resistance of cast aluminium matrix composites (A3xx. x/SiCp) in a humid environment, *Mater. Corros.*, 54 (2003) 311-317.
- [31] M. Mohedano, C. Blawert, M.L. Zheludkevich, Cerium-based sealing of PEO coated AM50 magnesium alloy, *Surf. Coat. Technol.*, 269 (2015) 145-154.
- [32] R. Arrabal, M. Mohedano, E. Matykina, A. Pardo, B. Mingo, M.C. Merino, Characterization and wear behaviour of PEO coatings on 6082-T6 aluminium alloy with incorporated α -Al₂O₃ particles, *Surf. Coat. Technol.*, 269 (2015) 64-73.
- [33] E. Matykina, R. Arrabal, P. Skeldon, G.E. Thompson, Investigation of the growth processes of coatings formed by AC plasma electrolytic oxidation of aluminium, *Electrochim. Acta*, 54 (2009) 6767-6778.
- [34] S. Aliasghari, T. Hashimoto, P. Skeldon, G. Thompson, Effect of Chloride Ions in Plasma Electrolytic Oxidation of Titanium, *ECS Electrochemistry Letters*, 3 (2014) C17-C20.
- [35] W. Xue, Features of film growth during plasma anodizing of Al 2024/SiC metal matrix composite, *Appl. Surf. Sci.*, 252 (2006) 6195-6200.
- [36] M. Liu, P.J. Uggowitzer, A.V. Nagasekhar, P. Schmutz, M. Easton, G.-L. Song, A. Atrous, Calculated phase diagrams and the corrosion of die-cast Mg–Al alloys, *Corros. Sci.*, 51 (2009) 602-619.
- [37] C.A. Nunez-Lopez, P. Skeldon, G.E. Thompson, P. Lyon, H. Karimzadeh, T.E. Wilks, The corrosion behaviour of Mg alloy ZC71/SiCp metal matrix composite, *Corros. Sci.*, 37 (1995) 689-708.
- [38] R. Arrabal, E. Matykina, T. Hashimoto, P. Skeldon, G.E. Thompson, Characterization of AC PEO coatings on magnesium alloys, *Surf. Coat. Technol.*, 203 (2009) 2207-2220.
- [39] J. Liang, L. Hu, J. Hao, Characterization of microarc oxidation coatings formed on AM60B magnesium alloy in silicate and phosphate electrolytes, *Appl. Surf. Sci.*, 253 (2007) 4490-4496.
- [40] C. Lim, S. Lim, M. Gupta, Wear behaviour of SiC p-reinforced magnesium matrix composites, *Wear*, 255 (2003) 629-637.
- [41] N. Chawla, Y.-L. Shen, Mechanical behavior of particle reinforced metal matrix composites, *Adv. Eng. Mater.*, 3 (2001) 357-370.
- [42] F. Labib, H. Ghasemi, R. Mahmudi, Dry tribological behavior of Mg/SiC p composites at room and elevated temperatures, *Wear*, 348 (2016) 69-79.
- [43] P.B. Srinivasan, C. Blawert, W. Dietzel, Dry sliding wear behaviour of plasma electrolytic oxidation coated AZ91 cast magnesium alloy, *Wear*, 266 (2009) 1241-1247.
- [44] H. Dong, Surface engineering of light alloys: aluminium, magnesium and titanium alloys, Elsevier 2010.
- [45] Y. Yang, H. Wu, Effects of Current Frequency on the Microstructure and Wear Resistance of Ceramic Coatings Embedded with SiC Nano-particles Produced by Micro-arc Oxidation on AZ91D Magnesium Alloy, *J MaterSci Technol*, 26 (2010) 865-871.

ACCEPTED MANUSCRIPT

Tables

Table I Vickers hardness of AZ91/SiC/0-10p.

Material	HV ₅
AZ91	82± 6
AZ91/SiC/2p	116±18
AZ91/SiC/5p	129± 10
AZ91/SiC/10p	133±4

Table II Surface roughness of PEO coated AZ91/SiC/0-10p-PEO.

Material	R_a (μm)	R_z (μm)
AZ91-PEO	2.1 ± 1.8	18.3 ± 0.8
AZ91/SiC/2p-PEO	3.6 ± 0.1	21.5 ± 1.0
AZ91/SiC/5p-PEO	6.8 ± 0.2	41.3 ± 1.0
AZ91/SiC/10p-PEO	7.4 ± 1.5	39.0 ± 1.5

Figure captions

Figure 1. (a) Experimental set-up for hydrogen evolution test and (b) detail of the working cell.

Figure 2. Scanning electron micrograph of (a) AZ91, (b,e,f) AZ91/SiC/2p, (c) AZ91/SiC/5p and (d) AZ91/SiC/10p.

Figure 3. Surface potential maps and potential profiles in selected areas of (a, b) AZ91 and (c, d) AZ91/SiC/5p.

Figure 4. Voltage/Current-time curves obtained during PEO process for AZ91/SiC/0-10p

Figure 5. Scanning electron micrographs with the locations of EDS analysis of the cross sections of (a,b) AZ91-PEO and (c,d) AZ91/SiC/10p.

Figure 6. X-ray diffraction patterns of PEO coated AZ91/SiC/0-10p composites.

Figure 7. SEM micrograph of a SiC particle partially oxidized and incorporated into the PEO coating.

Figure 8. Corrosion rate as a function of SiC_p vol. % calculated from H₂ evolution measurements.

Figure 9. Potentiodynamic curves after 1h of immersion in NaCl 3.5 wt. % for (a) AZ91/SiC/0-10p and (b) AZ91/SiC/0-10p-PEO. (c) Corrosion current density as a function of SiC_p vol. % for AZ91/SiC/0-10p and AZ91/SiC/0-10p-PEO.

Figure 10. Scanning electron micrographs of the cross sections after 8 d of exposure in NaCl 3.5

wt. % aqueous solution (a) AZ91 and (b,c) AZ91/SiC/5p.

Figure 11. Optical micrographs of the cross sections after 8 d of exposure in NaCl 3.5 wt. % aqueous solution AZ91/SiC/5p-PEO.

Figure 12. Mass loss as a function of the sliding distance for (a) uncoated AZ91/SiC/0-10p and (b) PEO coated AZ91/SiC/0-10p.

Figure 13. Track depth (a) and track width (b) as a function of SiC_p vol. % of uncoated AZ91/SiC/0-10p

Figure 14. Longitudinal and cross section scanning electron micrographs of the wear track of (a,b) AZ91 and (c,d) AZ91/SiC/10p.

Figure 15. (a)Cross section and (b) longitudinal scanning electron micrographs of the wear track of AZ91/SiC/2p-PEO.

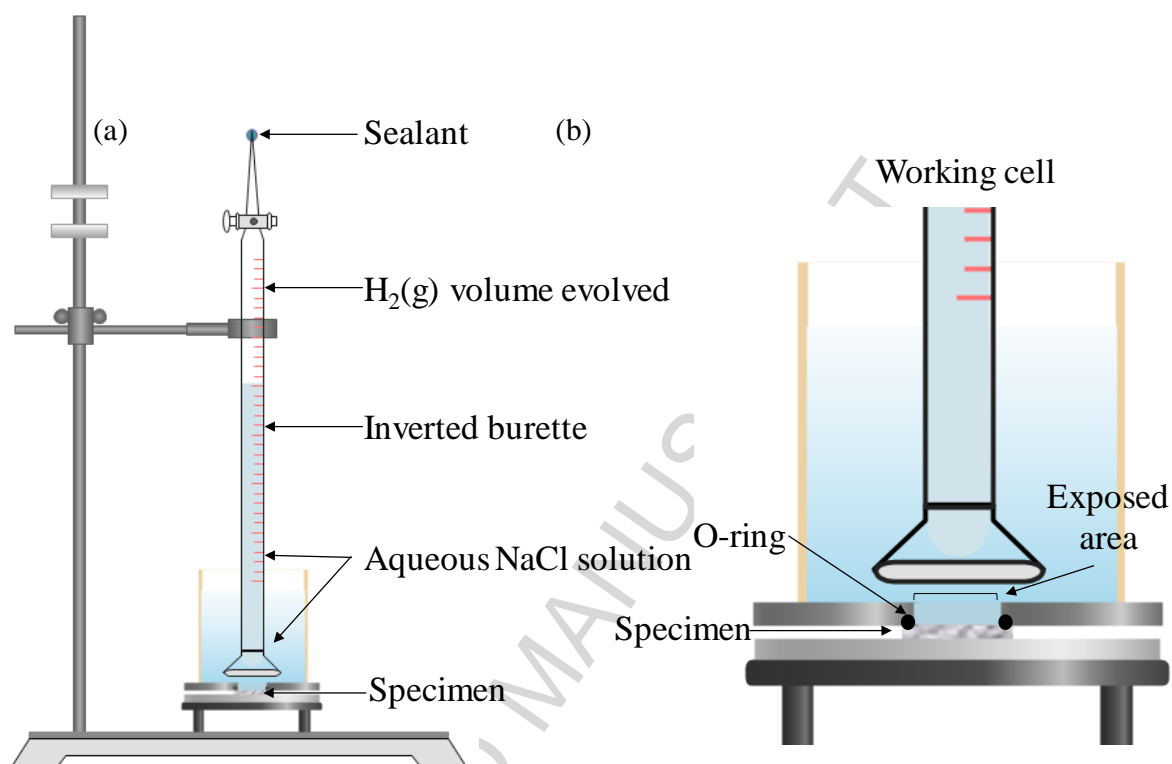


Figure 1

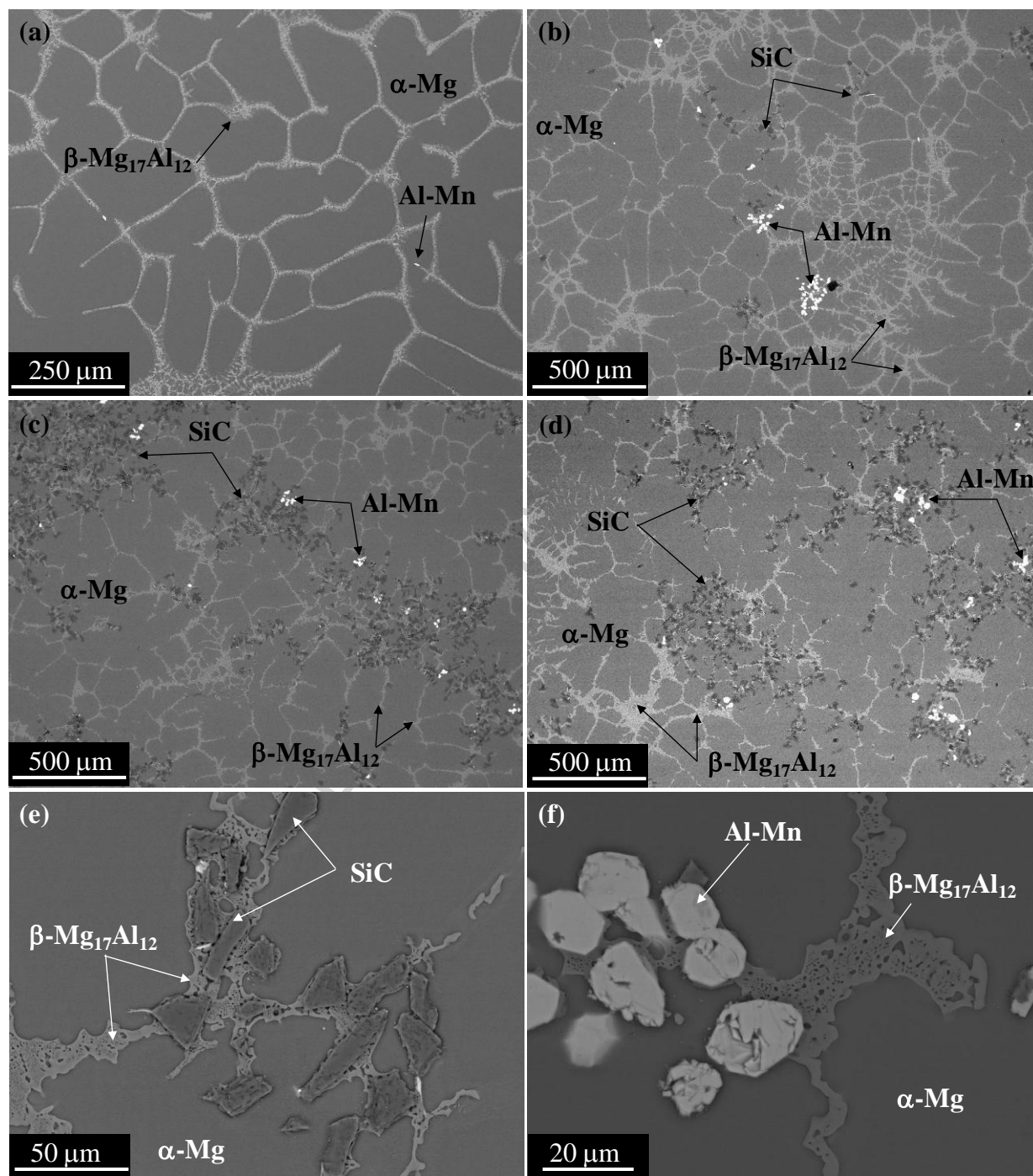


Figure 2

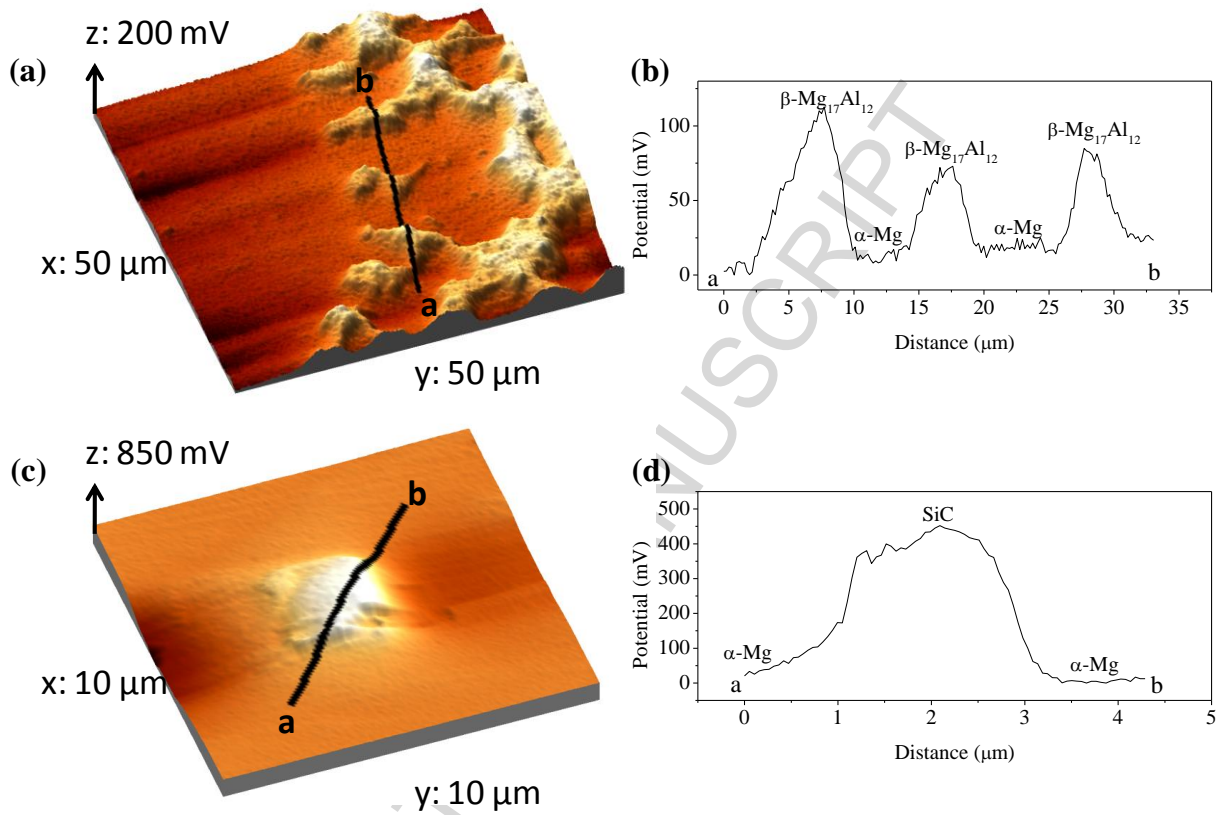


Figure 3

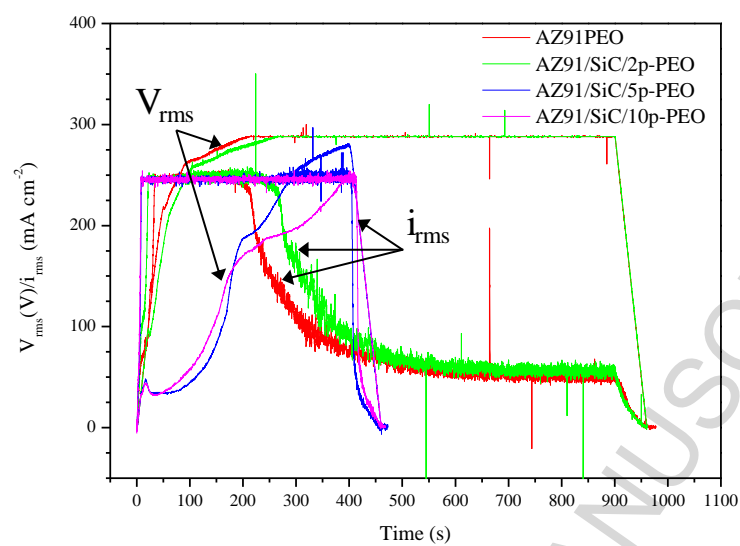


Figure 4

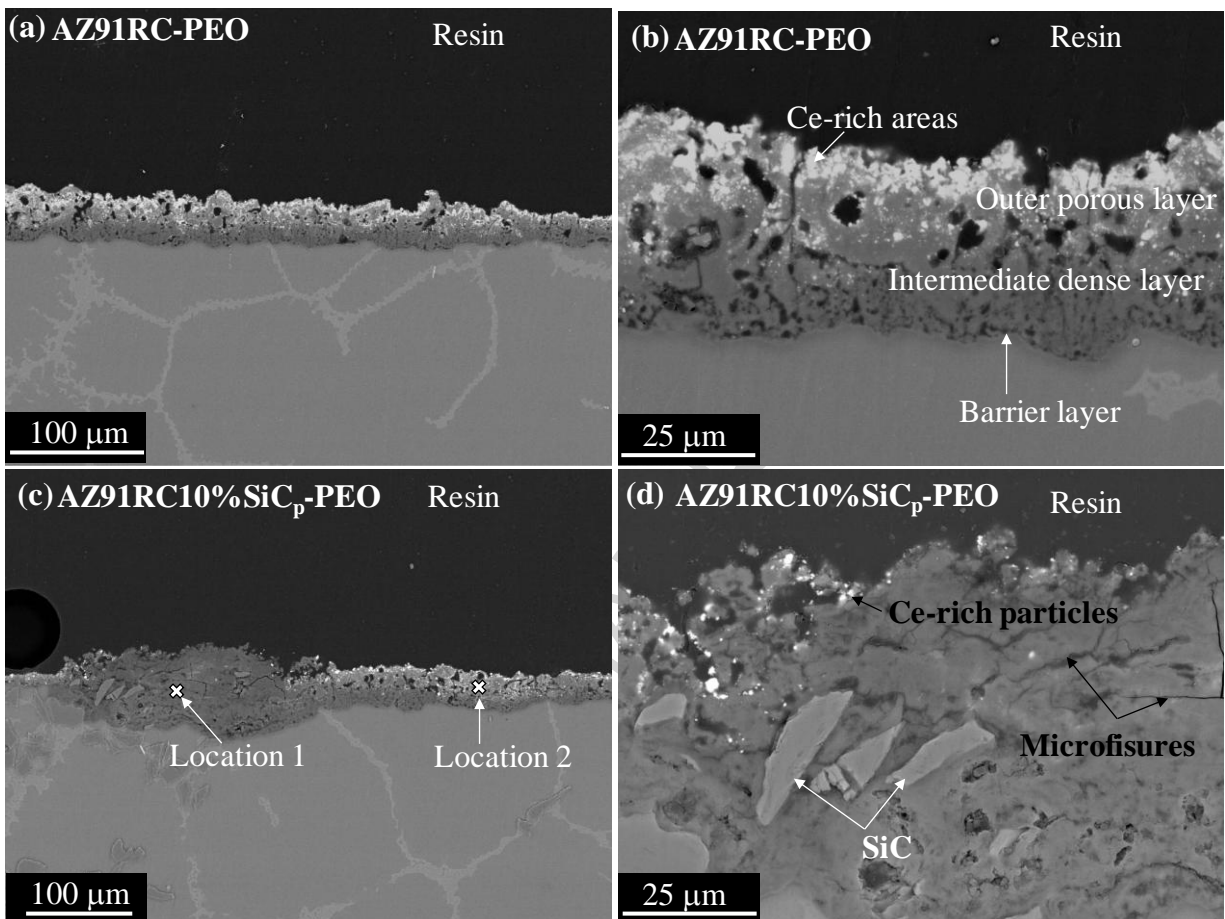


Figure 5

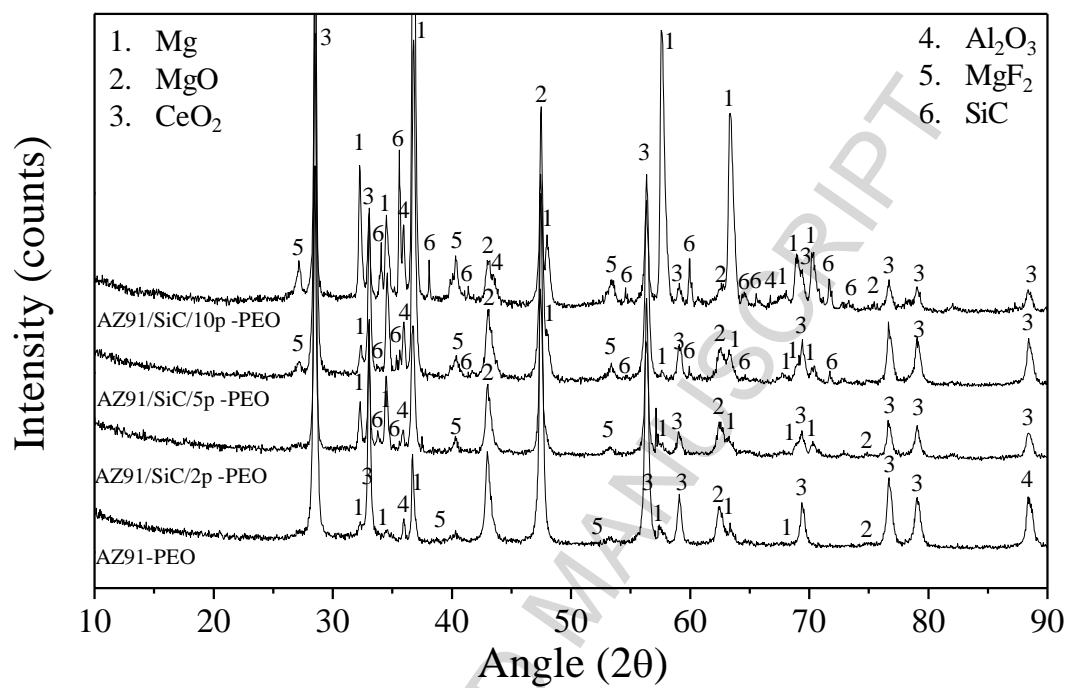


Figure 6

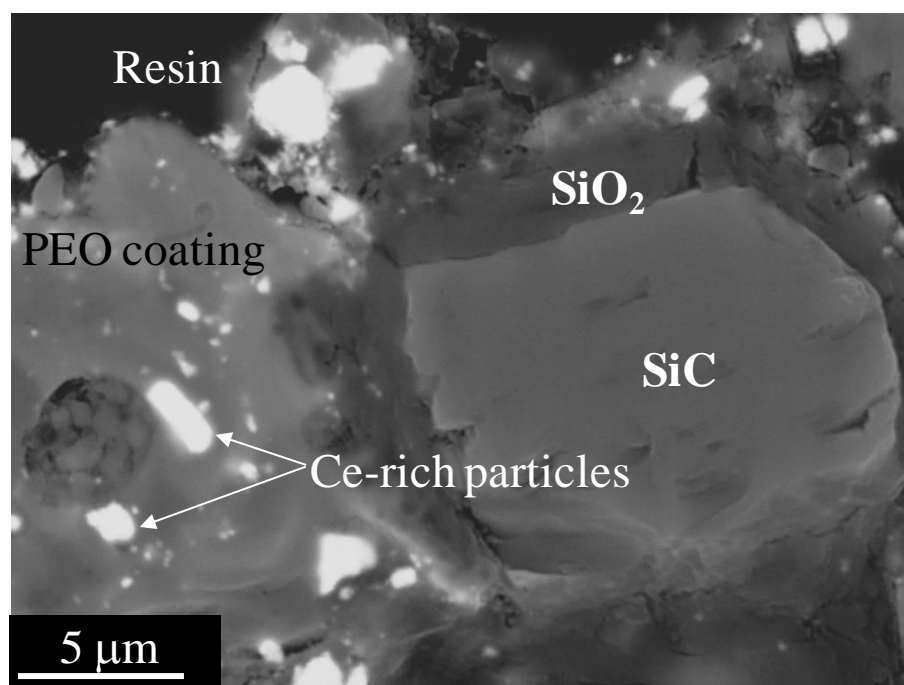


Figure 7

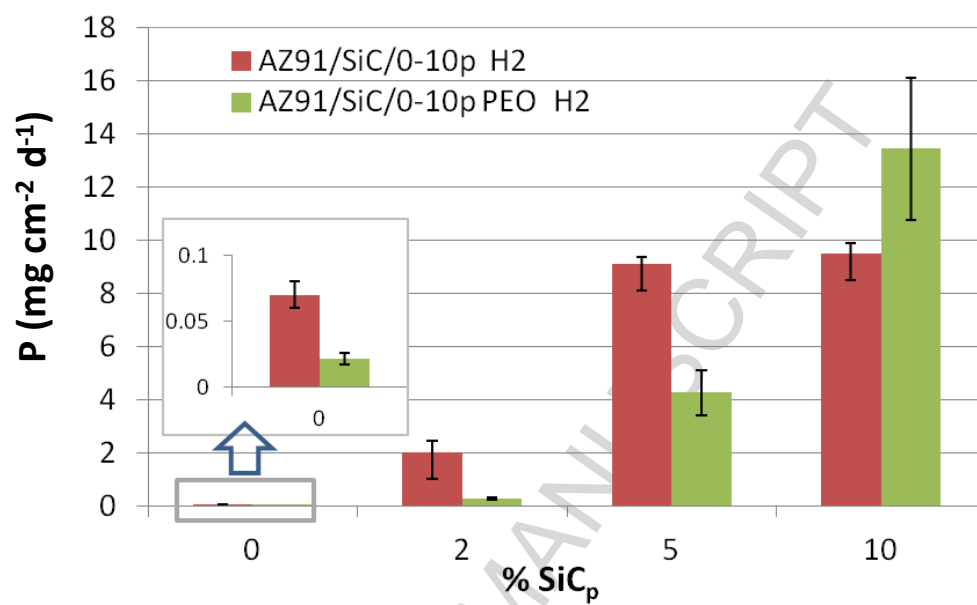


Figure 8

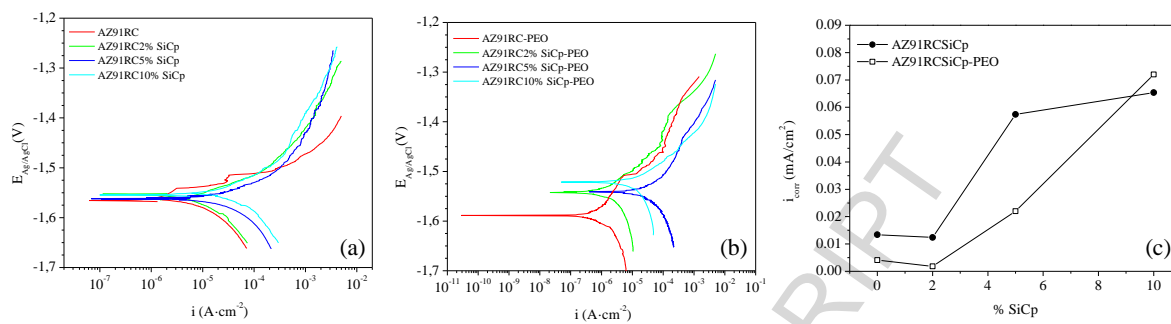


Figure 9

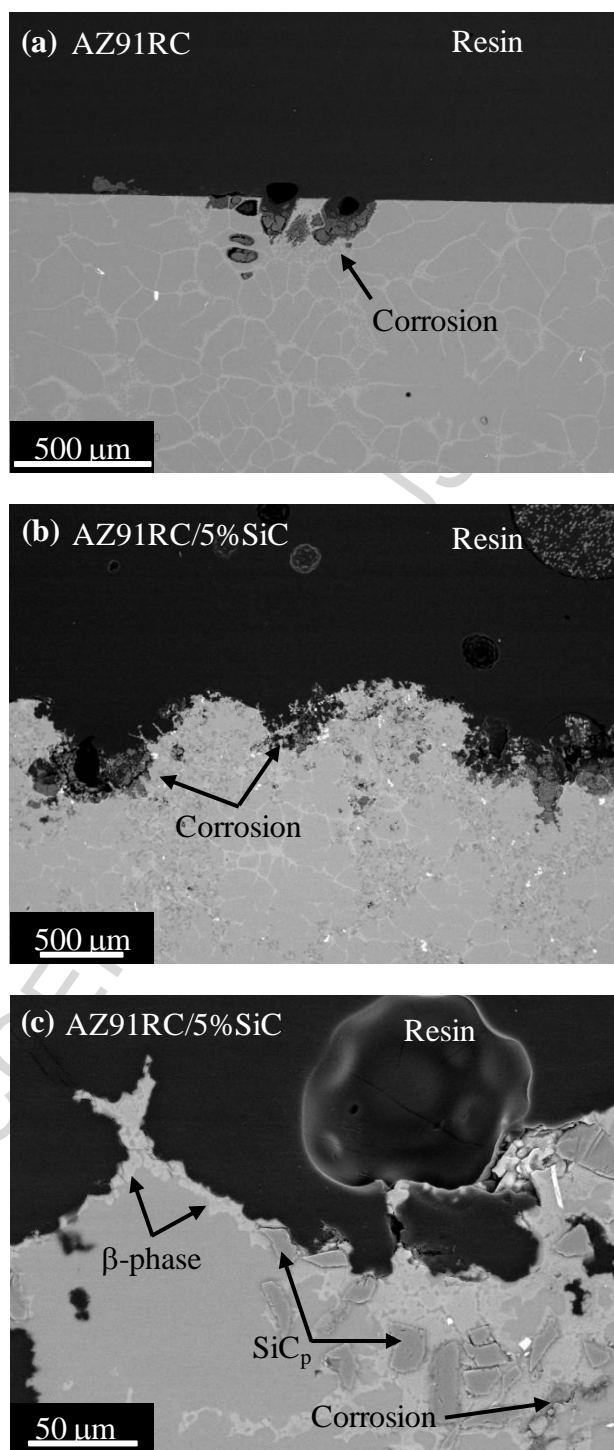


Figure 10

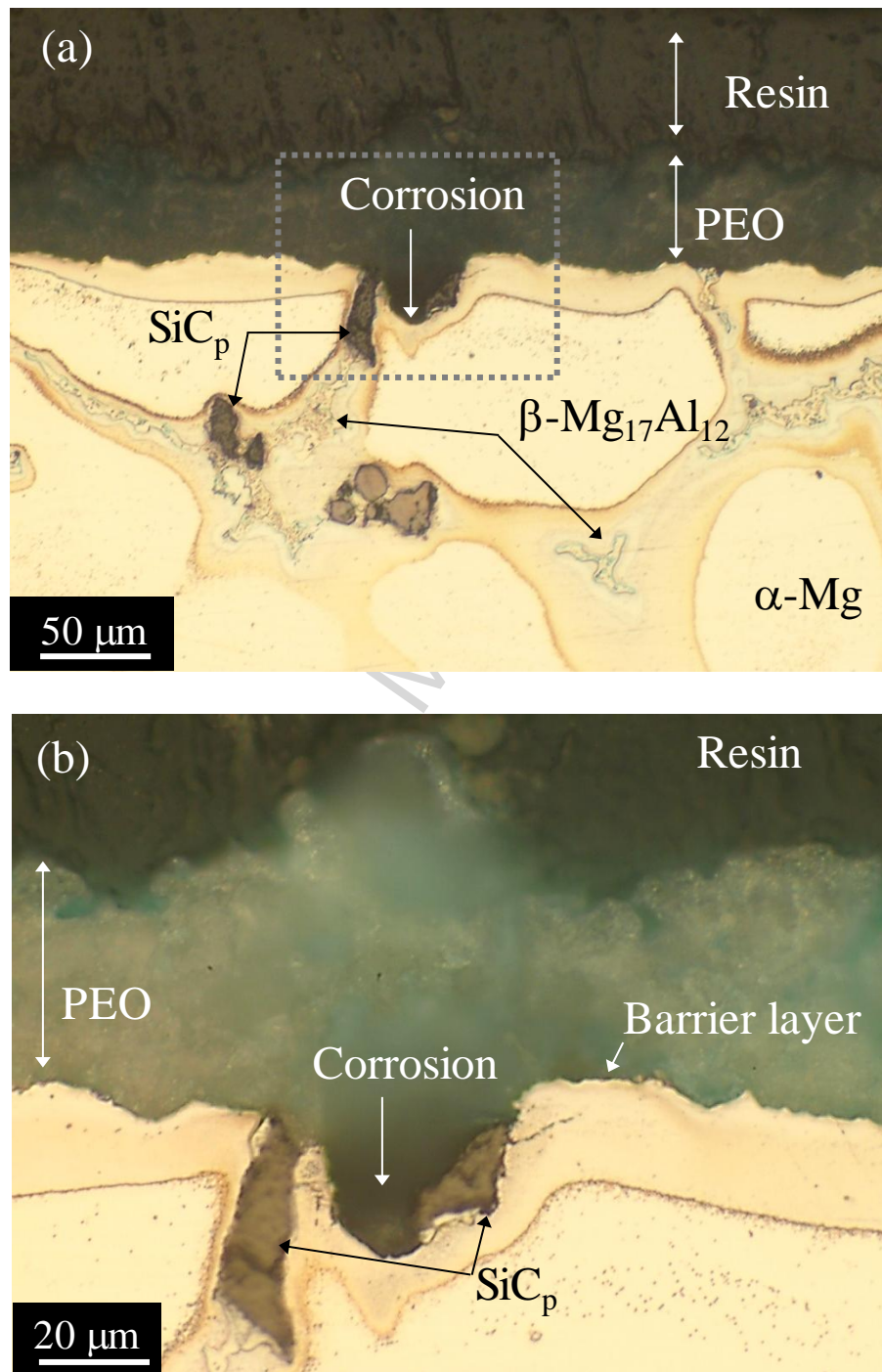


Figure 11

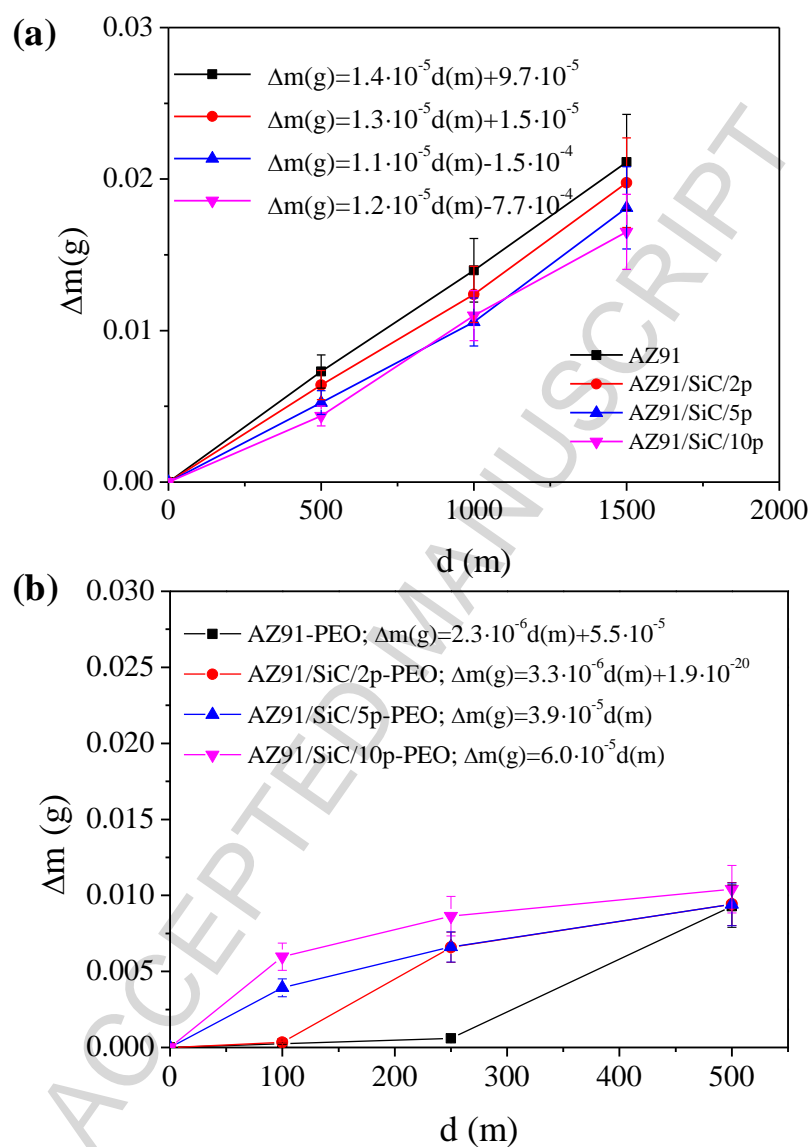


Figure 12

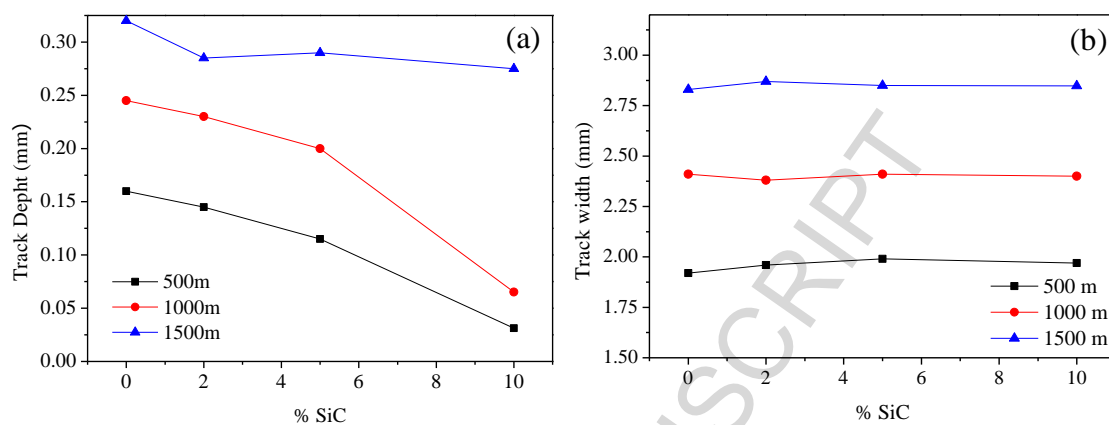


Figure 13

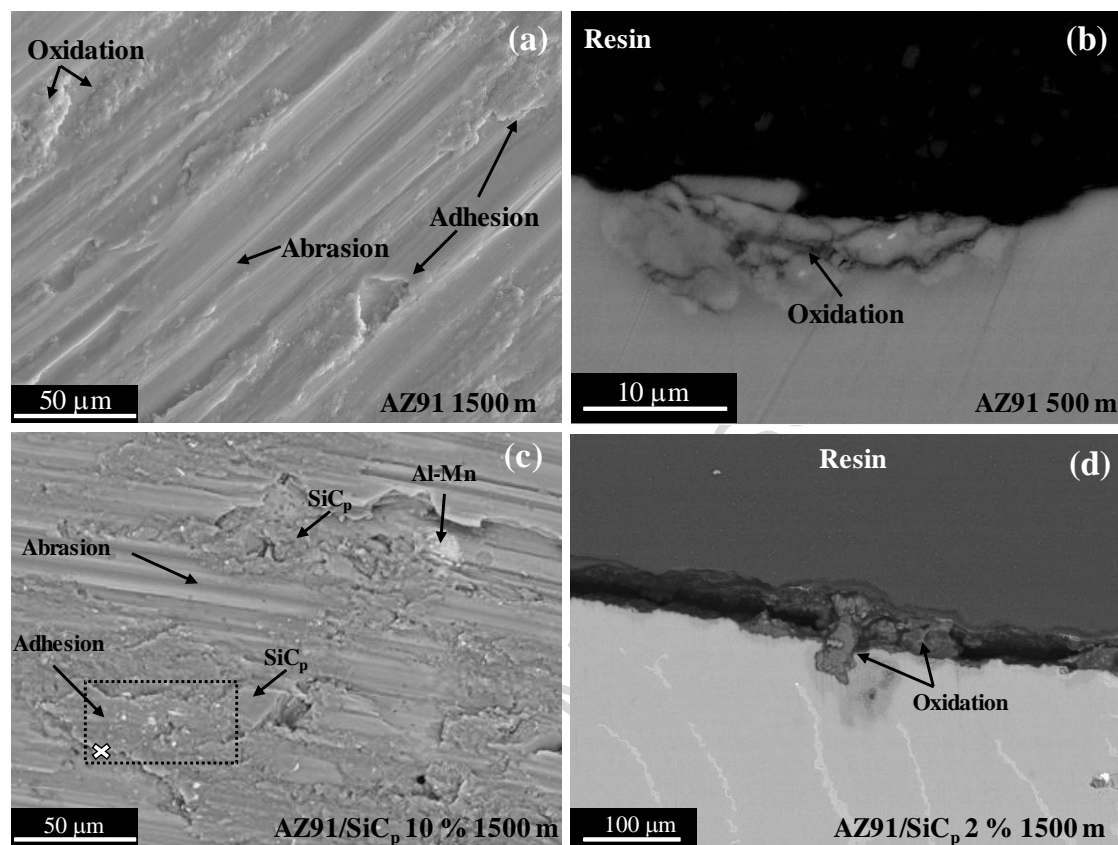


Figure 14

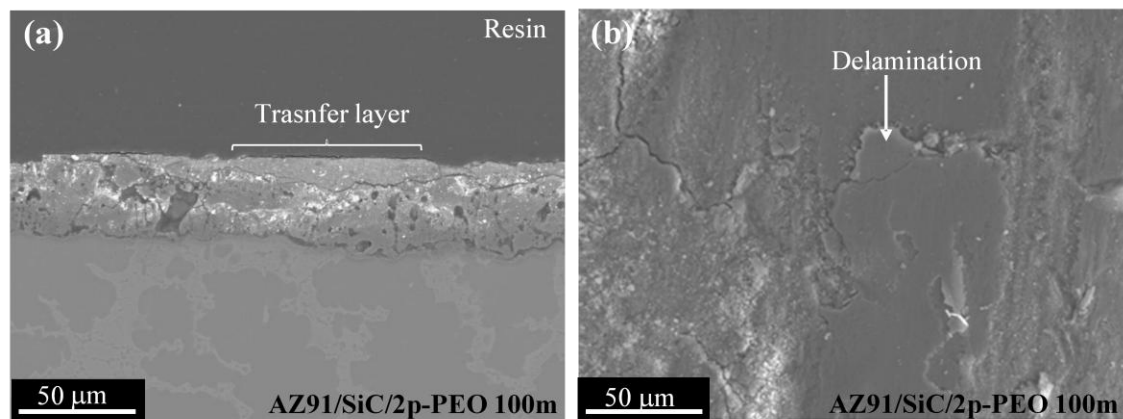


Figure 15

Highlights

- AZ91/SiC/0-10p corrosion rate increases with the volume fraction of reinforcement
- PEO coatings improve corrosion resistance of AZ91/SiC/0-10p composites
- PEO coatings corrosion rate increases with the volume fraction of SiC
- Wear resistance increases with SiC content in non-coated materials
- Wear behaviour of PEO coated materials is negatively influenced by SiC clusters